IEEE Journal of Microwaves

Received 4 March 2022; revised 14 April 2022; accepted 16 May 2022. Date of publication 10 June 2022; date of current version 7 July 2022.

Digital Object Identifier 10.1109/JMW.2022.3176283

Quantification of Exposure Level in a Reverberation Chamber for a Large-Scale Animal Study

RYOTA ITO[1], SANGBONG JEON[2], JIANQING WANG[1] (Fellow, IEEE), AE-KYOUNG LEE[2], JEONG-KI PACK[3], HYUNG-DO CHOI[1], YOUNG HWAN AHN[4,5], AND KATSUMI IMAIDA[6]

(Regular Paper)

[1]Graduate School of Engineering, Nagoya Institute of Technology, Nagoya, Aichi 466-8555, Japan
[2]Radio Technology Research Department, Electronics and Telecommunications Research Institute (ETRI), Daejeon 34129, Korea
[3]Department of Radio and Information Communication Engineering, Chungnam National University, Yuseong-gu, Daejeon 34134, Korea
[4]Department of Neurosurgery, Ajou University School of Medicine, Suwon 16499, Korea
[5]Neuroscience Graduate Program, Department of Biomedical Sciences, Graduate School of Ajou University, Suwon 16499, Korea
[6]Kagawa University, Takamatsu, Kagawa 760-8521, Japan

CORRESPONDING AUTHOR: Jianqing Wang (wang@nitech.ac.jp).

This work was supported in part by the Ministry of Internal Affairs and Communications, Japan, and in part by the ICT Research and Development Program of MSIT/IITP under Grant 2019-0-00102 (A Study on Public Health and Safety in a Complex EMF Environment), Republic of Korea.
This work involved human subjects or animals in its research. Approval of all ethical and experimental procedures and protocols was granted by the Animal Experimental Committee at the DIMS Institute of Medical Science, Inc., Japan, and the Korea Institute of Toxicology, the Institutional Animal Care and Use Committee under Approval No. IACUC 2004-0121.

ABSTRACT The US National Toxicology Program (NTP) conducted a long-term carcinogenic and toxicity study with small animals on the effects of mobile phone radiation at 900 MHz and 1900 MHz, respectively, and showed an increase in incidence of malignant schwannomas in the heart of male rats at very higher exposure levels. To verify and clarify the NTP study results, Japan and Korea are conducting a joint study using the same reverberation chamber type exposure system as in the NTP study. The purpose of this paper is to derive a quantitative relationship between the electric field strength in the reverberation chamber and the exposure level, i.e., the mean whole-body averaged specific absorption rate (WBA _ SAR) of rats based on a large-scale finite difference time domain (FDTD) simulation. First, two FDTD simulation methods, one with a single plane wave incidence and the other with simultaneous plane wave incidence, were compared, and then the former method was adopted for convenience and saving calculation time. The derived quantitative relationship between the WBA _ SAR and the electric field strength required to achieve the WBA _ SAR consists of a one-dimensional approximation model which considers only the body mass of rats and a two-dimensional approximation model which considers not only the body mass but also the number of rats. The two approximation models cover the entire two-year exposure period, and the exposure level in the two-year long-term exposure experiment is being well controlled. Moreover, unlike dosimetry in the NTP study, an uncertainty analysis of numerical dosimetry was performed in more details, and the combined standard uncertainty in the WBA _ SAR was found to be 16.1%.

INDEX TERMS Radio-frequency exposure system, reverberation chamber, dosimetry, specific absorption rate, animal study.

I. INTRODUCTION

The US National Toxicology Program (NTP) of the National Institute of Environmental Health Sciences (NIEHS) conducted a long-term carcinogenic and toxicity study with small animals on the effects of mobile phone radiation on code division multiple access (CDMA) and global system for mobile (GSM) communications at 900 MHz and 1900 MHz, respectively [1]–[4]. The results showed that the incidences

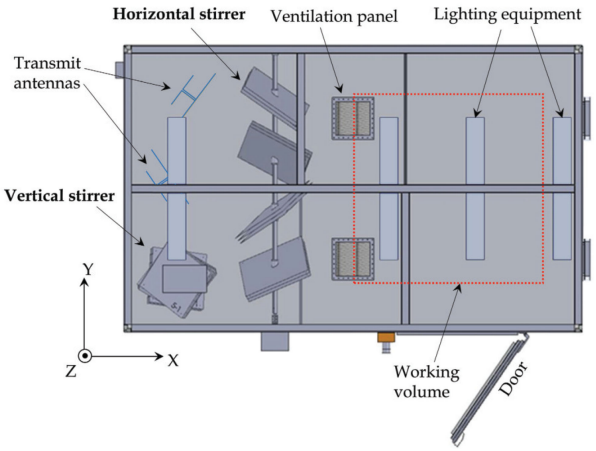

FIGURE 1. Structure of RC used in the replication experiment. The internal volume is 2.5 × 4.0 × 2.0 m^3. The working volume is 1.5 × 1.5 × 1.3 m^3.

of malignant schwannomas in the heart of male rats increased by both GSM and CDMA signals at very higher exposure levels that are not actually used. To verify and clarify the NTP study results, further reproducibility studies by other research organizations are expected [5] and [6]. Research teams in Japan and Korea are conducting a joint study for verification of the NTP study results, particularly on male rats, given limited research funding. A 900-MHz CDMA-modulated signal was selected for the radio-frequency (RF) exposure as it is used in mobile communication services in Japan and Korea. The experimental data in the two countries will be combined to increase the statistical power. This means that both countries must use the same exposure system and protocol.

The long-term NTP carcinogenicity study employed reverberation chambers (RC) to provide uniform RF exposure to rats and mice [7] and [8]. In a RC, since a large number of multipath waves are generated because of rotation of stirrers and reflection of radio waves by metal walls, the time variation of the real and imaginary terms (6 components) of the electric field (E-field) follows a normal distribution according to the central limit theorem. When RC is ideal, the time variation of each of the 6 components follows the same normal distribution, so the amplitude of each orthogonal component of the E-field follows a Rayleigh distribution and the phase follows a uniform distribution [9]. Since this is considered to be the same everywhere in the RC, the time variation of the E-field amplitude is considered to follow the same Rayleigh distribution regardless of the location in the RC. Therefore, the time average of the E-field strength is a constant value regardless of the location. This is why RC can provide a uniform exposure level to the animals inside [10] and [11].

In the Japan and Korea joint study, we also employ RC in the exposure system because it is a replication study. The RC is equipped with two stirrers and two antennas inside a metal box as shown in Fig. 1 [12]. The two stirrers are built vertically and horizontally in the RC with internal dimensions of 2.5 × 4.0 × 2.0 m^3, and each stirrer is composed of four square flat metallic plates. The two antennas are patch types that resonate at 900 MHz for radiating the 900-MHz CDMA signal. The E-field uniformity has been measured to be within the mean ± 1.0dB and mean ± 2.3dB under the empty and the 80-rat-loaded conditions, respectively.

This paper aims to derive a quantitative relationship between the E-field in the RC and the exposure level, i.e., the whole-body averaged specific absorption rate (WBA _ SAR) of rats for the large-scale joint animal study. The approach is the same as for NTP study, but the RC's performance and dosimetry results are directly related to the reliability of the replication study and therefore should be disclosed. Sections II describes the calculation method and its validation. Section III and IV describe the exposure protocol, simulation models, and the verification of simulation results. Section V shows the approximation models that quantify the relationship between the E-field and the WBA _ SAR with the mean body mass and the number of exposed rats as parameters. Section VI concludes this paper. The main points that extended [8] of the NTP study are as follows. First, the FDTD simulation method used in both this study and the NTP study is further validated by another FDTD simulation method with simultaneous plane wave incidence considering different phases. Next, the FDTD-simulated spatial E-field distribution in the RC is validated by measurement. Finally, an uncertainty analysis of WBA _ SAR is performed and compared to [8].

II. CALCULATION METHOD AND VALIDATION

Finite difference time domain (FDTD) method is popular to calculate the WBA _ SAR. However, when the FDTD method is applied to RC, the multiple reflections on the metal walls result in unconvergent solutions or unrealistic calculation time. Therefore, a two-step method is usually used to quantify the WBA _ SAR in a RC [13]–[15]. This method is based on the assumption that the time average of the E-field strength is a constant value in the absence of exposed rats regardless of the location. That is to say, it can be considered that plane waves with constant amplitude and random phase arrive from multiple directions at the same time. In the two-step method, first, the E-field in the RC is measured in the presence of the exposed rats. Next, under the assumption that multiple plane waves with the measured E-field strength are incident to the rats from all directions, the WBA _ SAR of the rats at each plane wave incident is calculated by the FDTD method, and the WBA _ SAR of the rats in the RC is obtained from their average.

This method, however, does not consider the phase difference of multipaths that actually exist in RCs. To clarify whether or not the phase difference affects the calculated WBA _ SAR, we conducted two FDTD simulations in Step 2 of the two-step method and compared the resulting difference between the WBA _ SARs. One simulation (simulation method A) is to calculate the WBA _ SAR without considering the phase difference of multipaths. The other simulation (simulation method B) is to calculate the WBA _ SAR in the RC taking into account the phase difference of multipaths.

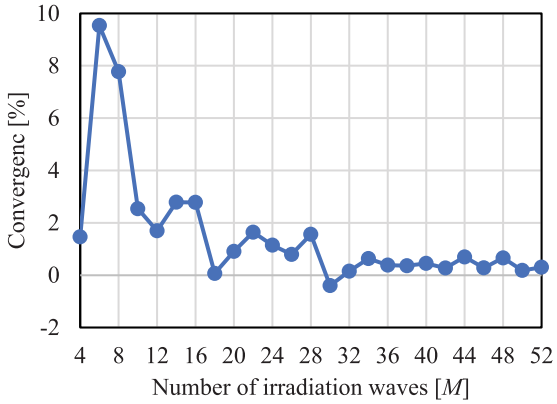

FIGURE 2. Convergence of the WBA _ SAR_A of rat versus the number of incident plane waves.

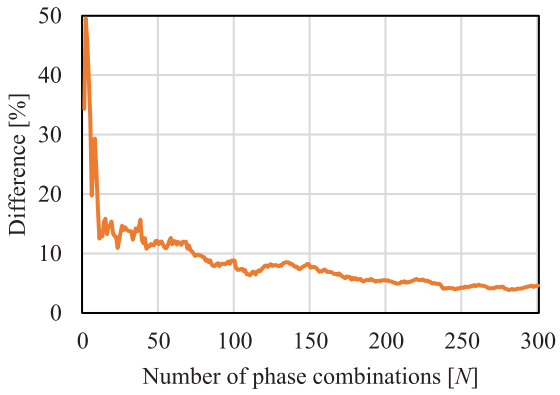

FIGURE 3. Difference between WBA _ SAR_A and WBA_SAR_B as the number of phase combinations *N* increases.

A. SIMULATION METHOD A - SINGLE INCIDENCE

In simulation method A, an anatomically based rat model was irradiated from $M/2$ directions, respectively, using a plane wave with an effective E-field strength E at 900 MHz. Considering transverse electric (TE) wave where the E-field is along latitude axis and the transverse magnetic (TM) wave where the E-field is along longitude axis in each direction, a total of M plane waves are incident. Then the SAR_m for each incident plane wave m ($m = 1, 2, \ldots M$) is calculated by

$$\mathrm{SAR_m} = \frac{\sigma}{\rho}|\mathrm{E_t}|^2 \tag{1}$$

where σ is the conductivity of tissue, ρ is the mass density of tissue, and E_t is the effective electric field strength inside tissue. It should be noted that the E-field can be divided into far-field and near-field. The IEEE and ICNIRP safety guidelines distinguish between the far-field case and near-field case. However, for SAR, as can be seen from Eq. (1), it is determined by the total E-field in the body. It does not matter if the E-field is a far-field or a near-field.

The phase difference between each plane wave was not taken into consideration, and the simulation was performed individually for each plane wave m. After obtaining the WBA _ SAR_m by M plane wave simulations, the rat WBA _ SAR is calculated by Eq. (2). This calculation method is defined as single incidence, and the calculated WBA _ SAR was named WBA _ SAR_A. In such a way, the rat WBA _ SAR is calculated by the simulation without considering the phase difference of each plane wave

$$\mathrm{WBA\_SAR_A} = \frac{\Sigma_{\mathrm{m=1}}^{\mathrm{M}}\mathrm{WBA\_SAR_m}}{\mathrm{M}} \tag{2}$$

where the subscript A means the single incidence.

In order to perform the simulation under an ideal RC environment, it is necessary to consider enough incident directions by setting an appropriate number of incident waves in the FDTD simulation. Fig. 2 shows the convergence of WBA _ SAR_A as a function of the number of incident waves for an anatomically based male rat model (described later) at 900 MHz. The rat model was irradiated with $M/2$ TE waves and $M/2$ TM waves, and M was changed from 4 to 52. It can be seen that the calculated WBA _ SAR_A converges as the number of incident plane waves M increases. When M exceeds 30, the WBA _ SAR_A convergences within $\pm 1\%$.

B. SIMULATION METHOD B - SIMULTANEOUS INCIDENCE

However, there are two differences between the actual RC and the above simulation method A.

1) In the actual RC, radio waves with random phases arrive from multiple directions due to the rotation of the two stirrers. But in simulation method A, each incidence is simulated at the same phase.
2) In the actual RC, the number of radio waves arriving at the same time is variable. But in simulation method A, the number of the incident plane waves is assumed to be a constant value.

Therefore, it is necessary to clarify whether the WBA _ SAR calculation in the simulation method A is valid without considering the different phases of multiple incident waves.

To simulate a more appropriate situation for RC, the FDTD simulation was performed with multiple plane waves (M=52) simultaneously incidence to the male rat model in random phases. At this time, in order to consider various phase combinations, N patterns of the phase combinations were generated, and each was simulated to calculate the WBA _ SAR of rat. After that, WBA_SAR_B (the subscript B means the simultaneous incidence) was calculated by averaging with the number of phase combinations N. This result is compared with WBA_SAR_A obtained by the single incidence in simulation method A.

Fig. 3 shows the difference between WBA _ SAR_A and WBA_SAR_B as the number of phase combinations N increases. As the number of phase combinations N increases, the difference becomes smaller and convergence within 5% can be confirmed if N exceeds 200. From this result, it can be considered that the WBA_ SAR in the RC where the two stirrers produce a sufficient number of incident waves with different phases can be calculated by incidence of many single plane waves without considering their phases.

TABLE 1. Summary of Random Phase Combinations and Corresponding $|E|^2$

Combination	θ	$\lvert E\rvert^2$ or $\mathrm{WBA\_SAR_S}$
1	$\theta_i^1 - \theta_j^1$	$\mathrm{M} + 2\sum_{i=1}^{M-1}\sum_{j=i+1}^{M}\cos(\theta_i^1 - \theta_j^1)$
2	$\theta_i^2 - \theta_j^2$	$\mathrm{M} + 2\sum_{i=1}^{M-1}\sum_{j=i+1}^{M}\cos(\theta_i^2 - \theta_j^2)$
...	...	...
N	$\theta_i^N - \theta_j^N$	$\mathrm{M} + 2\sum_{i=1}^{M-1}\sum_{j=i+1}^{M}\cos(\theta_i^N - \theta_j^N)$

C. MONTE CARLO VALIDATION

To compare the two simulation methods, further verification was performed using Monte Carlo method. The Monte Carlo method is a method for probabilistically solving a phenomenon to be simulated by giving a sufficient random number to the input and observing the output value. In the RC, under the assumption that the effective E-field strength (simply, E-field strength) of each incident plane wave is 1 V/m, the total E-field strength of multiple waves with different phases can be expressed as

$$|E| = \sqrt{M + 2\sum_{i=1}^{M-1}\sum_{j=i+1}^{M}\cos(\theta_i - \theta_j)} \qquad (3)$$

where M is the number of incident waves, and θ_1 to θ_M follow an uniform distribution from $-\pi$ to π. Since the WBA _ SAR is proportional to the squared E-field strength, we have

$$\mathrm{WBA\_SAR_B} \propto M + 2\sum_{i=1}^{M-1}\sum_{j=i+1}^{M}\cos(\theta_i - \theta_j) \qquad (4)$$

The uniformity of the spatial E-field distribution in the RC is affected by the number of rotation steps of the stirrers. The number of rotation steps N corresponds to the total number of changes in the position of the stirrers. Assuming that the RC is ideal, the variation in the amplitude of the E-field at a certain location with the rotation of the stirrers should follow the Rayleigh distribution. In order to consider various phases, we generated N ($n = 1, 2, \ldots N$) random phase combinations between θ_i and θ_j. Substitute each phase combination into Eq. (4), the value related to the $\mathrm{WBA\_SAR_B}$ for the n-th phase combination can be obtained as shown in Table 1. Then the value related to the mean $\mathrm{WBA\_SAR_B}$ can be obtained from the average of the N values.

On the other hand, also assuming that the effective E-field strength is 1 V/m for each single plane wave incidence, the $\mathrm{WBA\_SAR_A}$ for M single plane wave incidence satisfies

$$\mathrm{WBA\_SAR_A} \propto M \qquad (5)$$

Then the difference between the $\mathrm{WBA\_SAR_A}$ and the $\mathrm{WBA\_SAR_B}$ can be calculated as

$$\mathrm{Diff.} = \frac{(\mathrm{WBA\_SAR_A}) - (\mathrm{WBA\_SAR_B})}{\mathrm{WBA\_SAR_B}}\%. \qquad (6)$$

Fig. 4 shows the difference between the two WBA _ SARs versus the number of the phase combinations N by Monte Carlo test. The number of the incident waves M was fixed at 52. The two red auxiliary lines correspond to the difference of +5% and -5%, respectively. When the number of phase combinations N is small, the difference between the single incidence $\mathrm{WBA\_SAR_A}$ and the simultaneous incidence $\mathrm{WBA\_SAR_B}$ varies greatly. However, it becomes smaller as the number of phase combinations N increases. When N exceeds 500, the difference between the two simulation methods is almost within ±5%. So, the Monte Carlo test shows the same result as the FDTD simulated one in Fig. 3.

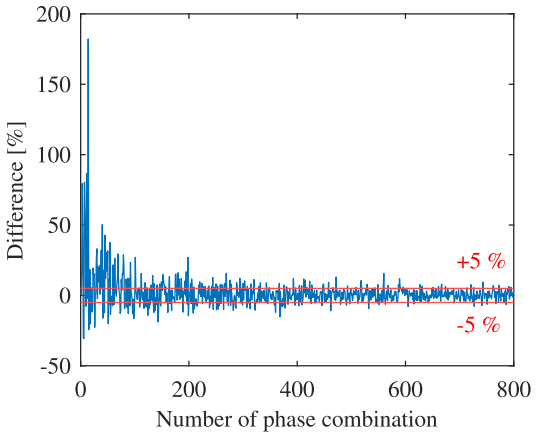

FIGURE 4. Difference between $\mathrm{WBA\_SAR_A}$ and $\mathrm{WBA\_SAR_B}$ as the number of phase combinations N increase. The number of incident waves M is fixed at 52.

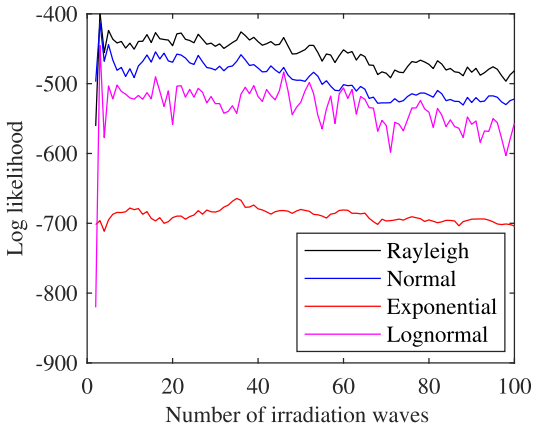

FIGURE 5. Log-likelihood of the E-field versus the number of incident waves M. The number of phase combinations N is set at 500.

In addition, Fig. 5 shows the number of incident waves on the horizontal axis and the log-likelihood of E-field strength on the vertical axis. For each number of incident waves, the log-likelihoods of the E-field strength approximated by the Rayleigh distribution, normal distribution, lognormal distribution, and exponential distribution are plotted. The higher the log-likelihood, the higher the approximation is. In Fig. 5, the Rayleigh distribution has the maximum log-likelihood, which is in line with the theory of RC.

Therefore, instead of calculating the WBA _ SAR in the RC considering the simultaneous incidence of multiple waves with different phases, it is valid to calculate the WBA _ SAR for single incidence without considering the phase difference.

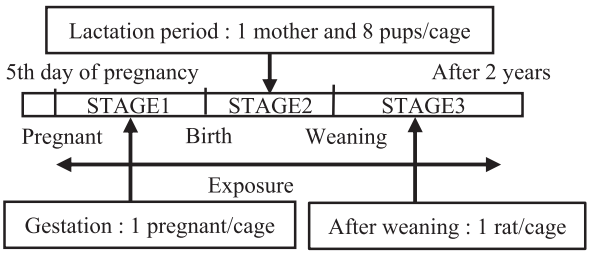

FIGURE 6. Exposure protocol of verification experiment.

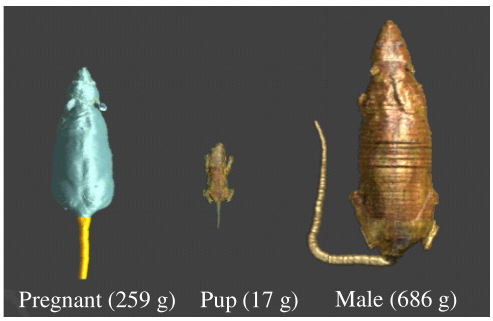

FIGURE 7. Original rat models.

The latter is more time-saving because it does not need to consider various phases. This conclusion is consistent with the consideration that the WBA _ SAR is a power-related quantity and power is phase independent. In the following simulations, we therefore adopt the simulation method A and set $M = 52$ to ensure a sufficient convergence.

III. EXPOSURE PROTOCOL AND SIMULATION MODELS

A. EXPOSURE PROTOCOL

The two-year NTP replication experiment using 900 MHz CDMA signals began in November 2020 in Japan and Korea. It will end in December 2022. Fig. 6 shows the protocol of the verification experiment. In the verification experiment, the rats are exposed at 4 W/kg WBA _ SAR, which is much higher than mobile phone exposure. The exposure began on the 5th day of pregnancy. Stage 1 is the gestation period. 30 pregnant rats, each in one cage, are exposed. Stage 2 is the lactation period. Each cage has one mother rat and 8 pups. When 8 or more pups are born, eight are randomly selected with priority given to males. When less than 8 pups are born, the mother's pups that give birth to 8 or more are added as foster pups to 8 pups. Stage 3 is the post-weaning period. From weaning to adulthood, a total of 75 or 70 rats are exposed, one in each cage for two years.

B. RAT MODELS

In the FDTD simulations, three types of anatomically based rat models are used: pregnant rat model, pup rat model, and male rat model, for simulating the experimental environment at each stage of the protocol. Original pregnant, pup and male rat models are provided by IT'IS Foundation, as shown in Fig. 7. For exposure to pregnant rats at stage 1, the original pregnant rat model is scaled up to 300 grams. For exposure to mother rats and pups at stage 2, a scaled-down 300-gram adult rat model and eight scaled-up 30-gram pup models are used. For exposure at stage 3, rat models for simulating the rat growth from weaning to two years old are produced from scale-ups from the pup rat model or scale-up/scale-down from the male rat models. When the rat weighs 100 grams or less, the pup model is scaled up, and when the rat weighs 100 grams or more, the male rat model is scaled down. Tables 2 and 3 shows the outline of the models used at each stage.

TABLE 2. Rat Models Used at Stage 1 and Stage 2

Stage	1	2	
Model	Pregnant	Adult	Pup
Mass [g]	300	300	30
Length without tail [mm]	180	200	80

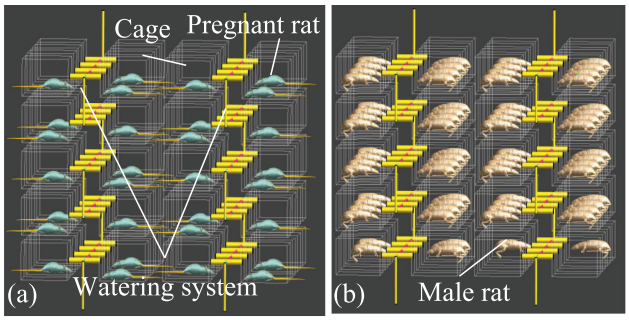

FIGURE 8. (a) Stage 1: 30 pregnant rats to be exposed. (b) 70 male rats to be exposed.

C. PLACEMENT OF RAT MODELS

During the exposure experiment, the rats are housed in cages installed in a rack. A water supply system which supplies water to the rats is attached to the rack. The cages are made of polycarbonate, and the racks are made of low loss fiber glass. The materials have little effect on the E-field, while the water supply system (except for the nozzles) is made of metal which cannot be ignored in the FDTD simulation. At stage 1 and stage 3, there is one rat model in each cage. At stage 2, a mother rat model and eight pup models are placed in each cage. Fig. 8 shows the placement of the rat models at stage 1 and stage 3, including the rack and water supply system. The distance between adjacent rats is determined based on the result in [16]. There are 30 pregnant rat models at stage 1, and 75 male rat models for weights of 450 grams or less and 70 male rat models for weights of 450 grams or more at stage 3. At stage 2, there are 30 mother rat models and 240 pup models. Since pups move randomly during stage 2, which affects the WBA _ SAR to some extent, two patterns of rat placement at stage 2 are assumed to be for pups that keep a distance from their mother and for pups that are close their mother, as shown in Fig. 9.

TABLE 3. Rat Models Used at Stage 3

Stage	3												
Model	Scaled-up from pup					Scaled-down or scaled-up from male							
Mass [g]	50	65	80	95	100	100	150	200	250	350	450	550	700
Length without tail [mm]	95	105	110	115	120	140	160	175	190	210	230	245	266

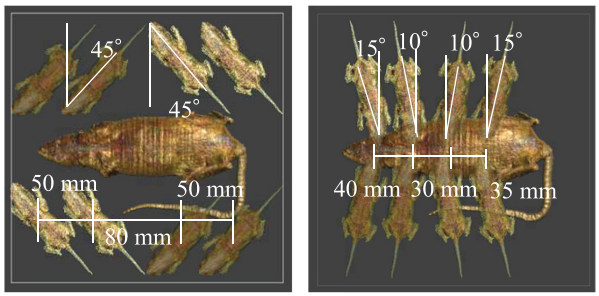

FIGURE 9. Two patterns of the rat placement at stage 2. (a) Pups keep a distance from their mother. (b) Pups close their mother.

IV. VERIFICATION OF SIMULATION

A. E-FIELD COMPARISON WITH MEASUREMENT

The spatial E-field strength distribution in our RC was measured and compared with the simulated spatial E-field strength distribution to verify the validity of the FDTD simulation. During the measurement, the vertical stirrer was set to 5 revolutions per minute (rpm), and the horizontal stirrer was set to 3 rpm. This combination of rotation was based on the trial and error measurements described in [12] and provided reasonable spatial E-field uniformity. Instead of actual rats, 75 330-gram water bottles were used and arranged as in stage 3. The water bottles were cylindrical. They were not completely rat-shaped but resembled the body shape of a rat. Such bottle models were also adopted in [8]. The permittivity of water is similar to that of high-water-content biological tissue, but the conductivity is different. When evaluating the SAR, using water bottles instead of rats is not a good choice due to the difference in conductivity. The rat model with a tail also affects the WBA _ SAR. Therefore, we adopted anatomically based rat models with tails in the SAR simulations. However, the purpose of this measurement using water bottles was to evaluate the uniformity of the spatial E-field distribution when the RC was loaded with lossy dielectric objects. From this point of view, this approach is acceptable as long as the FDTD simulation data used for comparison are also from the same bottle models.

For measurement, as shown in Fig. 10, the spatial E-field strength was measured at 150 ($5 \times 5 \times 6$) locations within the working volume ($1.5 \times 1.5 \times 1.3$ m^3). The distance between the measurement locations was approximately 0.375 m in the horizontal direction and 0.260 m in the vertical direction. The spatial E-field strength at each location was obtained as an average within 60 seconds. This was also based on the trial and error measurements. RC is known to provide a time-varying E-field whose time average depends on the number of

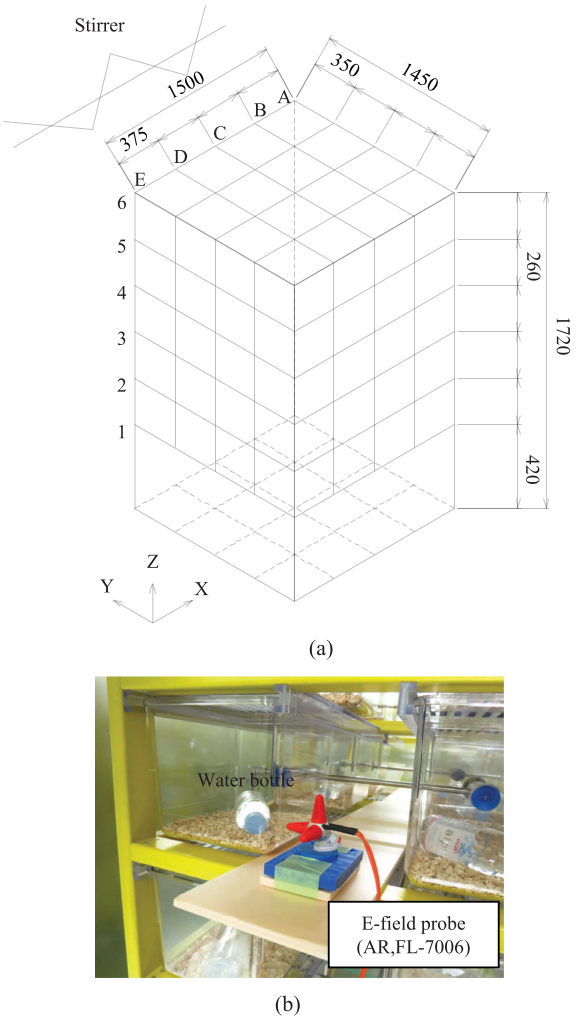

FIGURE 10. (a) Measurement locations in the RC. The unit is mm in the figure. (b) Measurement scenery with a three-axis E-field probe.

different phase combinations of incident waves. If the numbers are large enough, the average E-field will converge to a constant level, as shown in Fig. 4. Our measurements showed that the combination of 5 rpm for the vertical stirrer and 3 rpm for the horizontal stirrer is sufficient to converge within 60 seconds. That is to say, there is no significant difference between the E-field strength averaged within 60 seconds and 360 seconds. To save time, we therefore used the 60 s average as the spatial E-field strength. On the other hand, in the FDTD simulation, the male rat models was replaced by 330-gram water bottle models as used in the measurement, and the spatial E-field strength was calculated at the same 150 locations.

Fig. 11 shows the simulated and measured E-field strength at the 150 measurement locations. They were normalized to

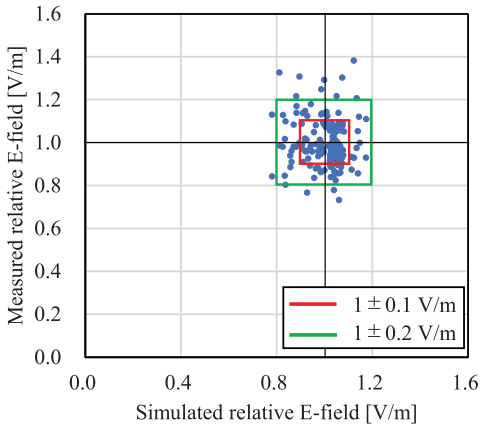

FIGURE 11. Comparison of the E-field strength simulated and measured at the 150 measurement locations.

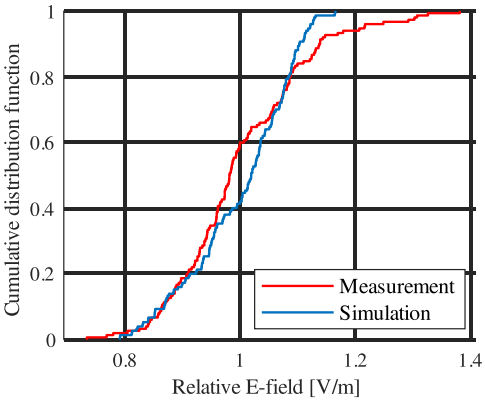

FIGURE 12. Cumulative density function of the E-field strength simulated and measured at the 150 measurement locations.

their mean values, respectively. The red square shows the range of ±10% of the mean value, and the green square shows the range of ±20% of the mean value. As can be seen, at 90.7% measurement locations, both the simulated E-field strength and the measured E-field strength are within the normalized mean value ± 20%. Moreover, Fig. 12 shows the cumulative density function (CDF) of the spatial E-field strength simulated and measured at the 150 measurement locations. It can be seen that both have almost the same distribution from a statistical point of view.

In order to expose the rats to a more uniform E-field strength in the RC, rotation of the rat placement position is always performed every one or two weeks during the two-year exposure period. This means that the 75 rats will be placed at the 150 measurement locations with equal probability. Under this condition, the 150 simulated and measured E-field strength data can be rearranged from the minimum to the maximum, respectively, to form two data sets. The root mean square error (RMSE) of the square of the spatial E-field strength between the two data sets (i.e., the simulation and measurement) is then calculated as 7.8%, which suggests the uncertainty of the simulated WBA _ SAR versus the measured

TABLE 4. Comparison of FDTD Simulated Mean WBA _ SAR at 1 V/m Between Japan and Korea

Stage	Mass [g]	Number	WBA_SAR [μW/kg]	
			Japan	Korea
1, Pregnant	300	30	83.5	83.5
2, Mother	300	30	84.8	85.5
2, Pup	30	240	48.6	47.8
3, Male	50	75	77.3	76.4
3, Male	65	75	98.7	97.9
3, Male	80	75	118.5	120.7
3, Male	95	75	136.3	136.7
3, Male	100	75	141.4	140.3
3, Male	150	75	117.9	123.1
3, Male	200	75	90.6	92.1
3, Male	250	75	75.9	77.7
3, Male	350	75	66.5	65.9
3, Male	450	75	60.9	61.5
3, Male	450	70	62.7	62.0
3, Male	550	70	57.6	57.7
3, Male	700	70	51.5	51.7

WBA _ SAR because the WBA _ SAR is proportional to the square of the E-field strength. So, it is considered that the simulation properly simulates the actual RC environment, and the FDTD simulation results shown below should be valid.

B. WBA _ SAR COMPARISON

For further verification of the simulation, the mean WBA _ SAR of all rats at each stage was first calculated using the FDTD method under an incident E-field strength of 1 V/m by Japan and Korea groups, independently. Table 4 shows the simulation results of the mean WBA _ SAR at stage 1, stage 2, and stage 3. Since two rat placement patterns were considered at stage 2, the mean WBA _ SAR of stage 2 was calculated by a weighted average of 1/3 of the WBA _ SAR for pattern 1 and 2/3 of the WBA _ SAR for pattern 2, in view of the actual situation of the pups in the cage. As can be seen from Table 4, the difference in the simulated mean WBA _ SAR between Japan and Korea is almost negligible. The almost same results from the two independent simulations also support the validity of the simulated mean WBA _ SAR at each stage. In addition, the difference on WBA _ SAR between the scale-up and scale-down of the rat model is within 4.3%.

C. EFFECT OF BODY MOVEMENT ON MEAN WBA _ SAR

In the long term exposure, rats can move around in the cage and face various directions. The effect of rat movement on the mean WBA _ SAR was discussed in stage 3 by FDTD simulation. Three rat models that weights 80 grams, 350 grams and 700 grams, respectively, were examined. Each rat model was assumed to face in one of the 8 different directions (from A to H) as shown in Fig. 13. In stage 3, there are a total of 75 or 70 exposed rats. The FDTD simulation for calculating the mean WBA _ SAR was repeated three times, and the facing direction of each rat was randomly chosen from the 8 directions each time. Table 5 shows the calculated mean

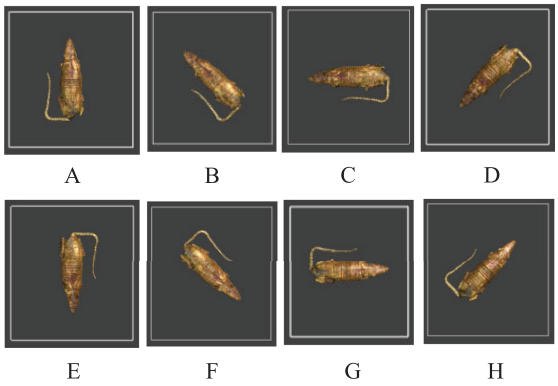

FIGURE 13. Rat models facing in various directions.

TABLE 5. Mean WBA _ SAR [μW/kg] at 1 V/m When the Rats Face Various Directions Due to Movement

Direction	80 g	350 g	700 g
Same	183.7	245.2	278.7
Random 1	187.9 (+2.3%)	245.1 (-0.0%)	276.6 (+0.8%)
Random 2	186.1 (+1.3%)	243.6 (-0.7%)	279.0 (+0.1%)
Random 3	184.8 (+0.6%)	244.7 (-0.2%)	277.0 (-0.6%)

WBA _ SAR at 1 V/m when all rats are facing the same direction (towards the water supply system) and when the rats are facing various directions randomly. The values in parentheses indicate the difference between the random direction and the same direction. It seems that the difference in the mean WBA _ SAR does not exceed $\pm 2.3\%$. So, the effect of rat movement on the mean WBA _ SAR is insignificant in the exposure experiment.

V. EXPOSURE LEVEL QUANTIFICATION

The quantitative relationship between the spatial mean E-field strength in the RC and the mean WBA _ SAR of rats is derived by the validated FDTD simulation at each stage. The mean WBA _ SAR of rats at each stage was first calculated under an E-field strength of 1 V/m. Then the mean WBA _ SAR and its standard deviation of the exposed rat models at each stage are obtained. In addition, the mean E-field strength required to achieve a WBA _ SAR target (4 W/kg in this study) is also derived as following based on the above simulation results.

$$E = \sqrt{\frac{\text{WBA\_SAR}_{\text{target}}}{\text{WBA\_SAR}|_{E=1\,\text{V/m}}}} \tag{7}$$

Using Eq. (7), the mean E-field strength to achieve a mean WBA _ SAR of 4 W/kg can be calculated from the simulated mean WBA _ SARs in Table 4. It is 218.9 V/m at stage 1 and 217.2 V/m at stage 2, respectively. At stage 3, the mean E-field strength to achieve 4 W/kg changes as the rats grow and gain weight. The blue circles in Fig. 14 show the mean WBA _ SAR versus the rat body mass at stage 3. Error bars indicate the standard deviation of the WBA _ SAR, which is within $\pm 9.6\%$ of the mean WBA _ SAR. This variation will be removed by changing the rat's location periodically to achieve

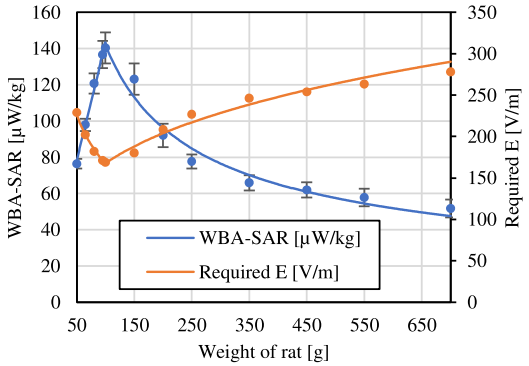

FIGURE 14. Mean WBA _ SAR and mean E-field strength to achieve 4 W/kg versus the rat body mass at stage 3.

a uniform exposure for all rats in the long term. The mean E-field strength to achieve the 4 W/kg WBA _ SAR is also shown in the figure with orange circles. A one-dimensional approximate model, plotted in Fig. 14 with a blue line, was obtained as

$$\text{WBA\_SAR} = \begin{cases} 1.3\times10^{-6}W + 1.34\times10^{-5} & W < 100\text{g} \\ 1.9\times10^{-3}W^{-0.563} & W \geq 100\text{g} \end{cases} \tag{8}$$

where W is the mean mass of the exposed rats. It can be seen that the approximation model gives a good fitting to the simulated mean WBA _ SAR. From this approximation model, the mean WBA _ SAR at any rat mass can be obtained, and the mean E-field strength to achieve the mean WBA _ SAR of 4 W/kg can be then calculated from (7) and plotted also in Fig. 14 with the orange line.

However, during the two-year long term exposure some rats may die for a variety of reasons. This reduces the number of exposed rats. For example, in the US NTP study, the survival probability of rats fell below 95 % at week 54, when the mean mass of rats was 594 grams. It is therefore necessary to derive a relationship between the mean E-field strength to achieve the 4 W/kg WBA _ SAR and both the mass of the rats as well as the number of rats. The mean WBA _ SAR of rats was further simulated when the rat mass exceeds 500 grams in stage 3 considering that the decrease in rat number occurs mainly in the late stage of the long term exposure.

Fig. 15 shows (a) the mean WBA _ SAR versus rat number and body mass for 1 V/m E-field strength, and (b) the mean E-field strength to achieve 4 W/kg WBA _ SAR versus rat number and body mass. As can be seen, as the number of rats decreases, the mean WBA _ SAR increases and the mean E-field strength to achieve 4 W/kg WBA _ SAR should also decrease. From this figure, we derived a two-dimensional approximation model by taking into account the number and mean body mass of rats as follows

$$\text{WBA\_SAR} = \text{aN}_\text{r}^2 + \text{bW}^2 + \text{cN}_\text{r}\text{W} + \text{dN}_\text{r} + \text{eW} + \text{f} \tag{9}$$

where W is the mean body mass and N_r is the number of rats. The coefficients a, b, c, d, e, and f were fitted as shown in Table 6.

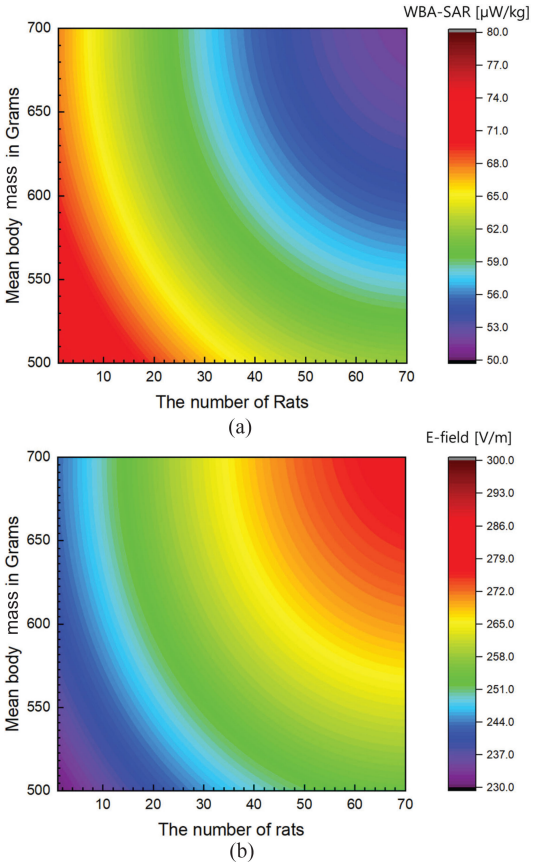

FIGURE 15. **(a) Mean WBA _ SAR versus rat number and body mass for 1 V/m E-field strength. (b) Mean E-field strength to achieve 4 W/kg versus rat number and body mass.**

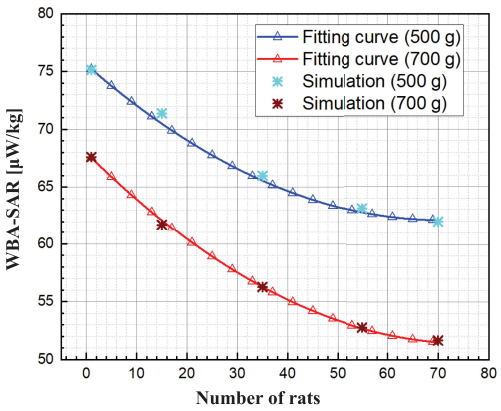

FIGURE 16. **Simulated and two-dimensional model approximated WBA _ SAR versus the number of exposed rats at the mean body mass of 500 grams and 700 grams.**

Fig. 16 compares the simulated and two-dimensional model approximated mean WBA _ SAR versus the number of exposed rats at the mean body mass of 500 grams and 700 grams. As can be seen, the two-dimensional approximation model gives a good fitting to the simulation results. Then the mean E-field strength to achieve 4 W/kg WBA _ SAR can be calculated from

$$E = \sqrt{\frac{4}{aN_r^2 + bW^2 + cN_rW + dN_r + eW + f}} \tag{10}$$

when the mean body mass of rats exceeds 500 grams.

In conclusion, if the mean body mass of rats is less than 500 grams, the mean E-field strength to achieve 4 W/kg WBA _ SAR is calculated from the one-dimensional approximation model which considers only the body mass (the number of rats is fixed). If the mean body mass of rats exceeds 500 grams, the mean E-field strength to achieve 4 W/kg WBA _ SAR is calculated from the two-dimensional approximation model which considers not only the body mass but also the number of rats.

The numerical uncertainties on WBA _ SAR are summarized in Table 7 based on the above analysis results. They include not only the effects of simulation methods and convergence, but also the effects of rat growth, rat mass, rat movement, and rat position in the RC. Unlike the uncertainty analysis in [8] which includes measurement-related uncertainties, the focus here is on the uncertainty of more detailed numerical dosimetry. From Table 7, the combined standard uncertainty of numerical dosimetry is 16.1% with respect to 24% in [8]. This uncertainty level seems reasonable given that the latter also includes measurement uncertainty. By the way, the measurement uncertainty in our study has been shown to be 0.63 dB for the E-field in [12], and therefore 15.6% for the WBA _ SAR. If we also include the E-field measurement uncertainty, the combined standard uncertainty should be 22.4%. Therefore, the dosimetry results in this replication study are almost the same as those in the NTP study.

TABLE 6. **Coefficient in the Two-Dimensional Approximation Model**

Coefficient	a	b	c
Value	2.684×10^{-9}	2.063×10^{-10}	-2.008×10^{-10}
Coefficient	d	e	f
Value	-2.806×10^{-7}	-2.853×10^{-7}	1.667×10^{-4}

TABLE 7. **Uncertainties in WBA _ SAR**

Component	Uncertainty
Single versus Simultaneous incidence	5.0%
Simulation convergence	1.0%
Simulation versus Measurement	7.8%
Rat model scalling	4.3%
Rat orientation due to movement	2.3%
Rat position in RC	9.6%
Rat body mass	7.6%
Combined standard uncertainty	16.1%

VI. CONCLUSION

Japan and Korea are conducting a joint study for verification of the US NTP study. The same RC-type exposure system is used in both countries. Since it is a replication study of the NTP study, the same dosimetry method was adopted in this study. However, compared to the dosimetry in the NTP

study [8], there are three points that extended the contents in [8]. First, the FDTD simulation method (single incidence) used in both this study and the NTP study has been validated by another FDTD simulation method with simultaneous incidence considering phases. Next, the FDTD-simulated spatial E-field distribution in the RC has been compared with the measured one, and the agreement between them has been quantitatively clarify. Both of these contribute to increasing the reliability of the numerical dosimetry results in both this study and the NTP study. Moreover, an uncertainty analysis of the WBA _ SAR has been performed. Unlike the uncertainty analysis in [8], the focus in this study is on the uncertainty of numerical dosimetry, which provides further insight into the uncertainty of FDTD-simulated WBA _ SAR. As a result, a quantitative relationship between the mean E-field strength in the RC and the exposure level, i.e., the mean WBA _ SAR of rats has been derived based on a large-scale FDTD simulation. The derived quantitative relationship consists of a one-dimensional approximation model which considers only the body mass of rats and a two-dimensional approximation model which considers not only the body mass but also the number of rats. The combined standard uncertainty in the mean WBA _ SAR has been found to be 16.1%. Using this quantitative relationship, the exposure level in the two-year long-term exposure experiment is being well controlled.

REFERENCES

[1] National Toxicology Program, "Toxicology and carcinogenesis studies in sprague dawley (hsd: Sprague dawley SD) rats exposed to wholebody radio frequency radiation at a frequency (900 MHz) and modulations (GSM and CDMA) used by cell phones," NC Nat. Toxicol. Program, Res. Triangle Park, NC, USA, Tech. Rep. NTP-TR-595, 2018, doi: 10.22427/NTP-TR-595.

[2] National Toxicology Program, "Toxicology and carcinogenesis studies in B6C3F1/N mice exposed to whole-body radio frequency radiation at a frequency (1,900 MHz) and modulations (GSM and CDMA) used by cell phones," NC Nat. Toxicol. Program, Res. Triangle Park, NC, USA, Tech. Rep. NTP TR-596, 2018, doi: 10.22427/NTP-TR-596.

[3] M. E. Wyde *et al.*, "Effect of cell phone radiofrequency radiation on body temperature in rodents: Pilot studies of the national toxicology program's reverberation chamber exposure system," *Bioelectromagnetics*, vol. 39, no. 3, pp. 190–199, Apr. 2018, doi: 10.1002/bem.22116.

[4] S. L. Smith-Roe *et al.*, "Evaluation of the genotoxicity of cell phone radiofrequency radiation in male and female rats and mice following subchronic exposure," *Environ. Mol. Mutagenesis*, vol. 61, no. 2, pp. 276–290, Feb. 2020, doi: 10.1002/em.22343.

[5] International Commission on Non-Ionizing Radiation Protection (ICNIRP), "ICNIRP note: Critical evaluation of two radiofrequency electromagnetic field animal carcinogenicity studies published in 2018," *Health Phys.*, vol. 118, no. 5, pp. 525–532, May 2020, doi: 10.1097/HP.0000000000001137.

[6] National Toxicology Program (NTP), "Cellphone radio frequency radiation studies," U.S. Dept. Health Human Services, Durham, NC, USA. [Online]. Available: https://ntp.niehs.nih.gov/whatwestudy/topics/cellphones/index.html

[7] M. H. Capstick *et al.*, "A radio frequency radiation exposure system for rodents based on reverberation chambers," *IEEE Trans. Electromagn. Compat.*, vol. 59, no. 4, pp. 1041–1052, Aug. 2017, doi: 10.1109/TEMC.2017.2649885.

[8] Y. Gong *et al.*, "Life-time dosimetric assessment for mice and rats exposed in reverberation chambers for the two-year NTP cancer bioassay study on cell phone radiation," *IEEE Trans. Electromagn. Compat.*, vol. 59, no. 6, pp. 1798–1808, Dec. 2017, doi: 10.1109/TEMC.2017.2665039.

[9] G. Kostas and B. Boverie, "Statistical model for a mode-stirred chamber," *IEEE Trans. Electromagn. Compat.*, vol. 33, no 4, pp. 366–370, Nov. 1991, doi: 10.1109/15.99120.

[10] C. L. Holloway, D. A. Hill, J. M. Ladbury, and G. Koepke, "Requirements for an effective reverberation chamber: Unloaded or loaded," *IEEE Trans. Electromagn. Compat.*, vol. 48, no. 1, pp. 187–194, Feb. 2006, doi: 10.1109/TEMC.2006.870709.

[11] J. Chakarothai, J. Wang, O. Fujiwara, K. Wake, and S. Watanabe, "Dosimetry of a reverberation chamber for whole-body exposure of small animal," *IEEE Trans. Microw. Theory Techn.*, vol. 61, no. 9, pp. 3435–3445, Sep. 2013, doi: 10.1109/TMTT.2013.2273761.

[12] S. Jeon *et al.*, "Field uniformity assessment of a reverberation chamber for a large-scale animal study," *IEEE Access*, vol. 9, pp. 146471–146477, 2021, doi: 10.1109/ACCESS.2021.3122120.

[13] J. Shi, J. Chakarothai, J. Wang, K. Wake, S. Watanabe, and O. Fujiwara, "Quantification and verification of whole-body-average SARs in small animals exposed to electromagnetic fields inside reverberation chamber," *IEICE Trans. Commun.*, vol. E97-B, no. 10, pp. 2184–2191, Oct. 2014, doi: 10.1587/transcom.E97.B.2184.

[14] J. Chakarothai, J. Shi, J. Wang, O. Fujiwara, K. Wake, and S. Watanabe, "Numerical techniques for SAR assessment of small animals in reverberation chamber," *IEEE EMC Mag.*, vol. 4, no. 1, pp. 57–66, Feb. 2015, doi: 10.1109/MEMC.2015.7098514.

[15] T. Wu, A. Hadjem, M.-F. Wong, A. Gati, O. Picon, and J. Wiart, "Whole-body new-born and young rats' exposure assessment in a reverberating chamber operating at 2.4 GHz," *Phys. Med. Biol.*, vol. 55, no. 6, pp. 1619–1630, Mar. 2010, doi: 10.1088/0031-9155/55/6/006.

[16] S. Jeon *et al.*, "Distances between rats in reverberation chambers used for large-scale experiments," *J. Electromagn. Eng. Sci.*, vol. 21, pp. 148–152, Apr. 2021, doi: 10.26866/jees.2021.21.2.14.

RYOTA ITO received the B.E. degree in electrical and mechanical engineering from the Nagoya Institute of Technology, Nagoya, Japan, in 2020, where he is currently working toward the master's degree in engineering. He is engaging in a numerical technique to simulate long-term RF exposure to rats in a reverberation chamber for his master's degree.

SANGBONG JEON received the B.S., M.S., and Ph.D. degrees in electronic engineering from Yeungnam University, Gyeongsan, South Korea, in 2001, 2003, and 2007, respectively. From 2008 to 2010, he was a Senior Research Engineer with the Korea Radio Promotion Association, Seoul, South Korea, where he conducted research in the fields of electromagnetic compatibility technology. Since 2010, he has been with the Radio and Satellite Research Division, Electronics and Telecommunications Research Institute, Daejeon, South Korea. His research interests include bio-electromagnetics and electromagnetic compatibility.

JIANQING WANG (Fellow, IEEE) received the B.E. degree in electronic engineering from the Beijing Institute of Technology, Beijing, China, in 1984, and the M.E. and D.E. degrees in electrical and communication engineering from Tohoku University, Sendai, Japan, in 1988 and 1991, respectively. He was a Research Associate with Tohoku University, and a Senior Engineer with Sophia Systems Company, Ltd. In 1997, he joined the Nagoya Institute of Technology, Nagoya, Japan, where he has been a Professor since 2005. He has authored the book *Body Area Communications* (Wiley-IEEE, 2012). His current research interests include biomedical communications and electromagnetic compatibility. He was the recipient of the IEEE EMCS Technical Achievement Award, in 2019.

AE-KYOUNG LEE received the B.S. and M.S. degrees in electronics and engineering from Chung-Ang University, Seoul, South Korea, in 1990 and 1992, respectively, and the Ph.D. degree in radio science and engineering from Chungnam National University, Daejeon, South Korea, in 2003. In 1992, she joined the Radio Technology Group, Electronics and Telecommunications Research Institute, Daejeon, South Korea, where she has been involved in projects on measurement technologies and numerical analyses of electromagnetic compatibility and human exposure to RF felds. She was the recipient of the Japan Microwave Prize at the 1998 Asia-Pacific Microwave Conference, Japan, and the Technology Award from the Korea Electromagnetic Engineering Society, in 1999.

JEONG-KI PACK received the B.S. degree in electronic engineering from Seoul National University, Seoul, South Korea, in 1978, and the M.S. and Ph.D. degrees in electromagnetic wave propagation from Virginia Tech, Blacksburg, VA, USA, in 1985 and 1988, respectively. From 1978 to 1983, he was a Researcher with the Agency for Defense Development, South Korea. In 1988, he joined ETRI, and moved to Dona-A University, Busan, South Korea, in 1989. Since February 1995, he has been a Professor with the Department of Radio Science and Engineering, Chungnam National University, Daejeon, South Korea, where he is currently an Emeritus Professor. His research interests include electro-magnetic wave propagation and bio-electromagnetics.

HYUNG-DO CHOI received the M.S. and Ph.D. degrees in material science from Korea University, Seoul, South Korea, in 1989 and 1996, respectively. Since 1997, he has been with the Electronics and Telecommunications Research Institute, South Korea. He has conducted research on the biological effects of RF radiation and has developed RF radiation protection standards and regulations. His current research interests include spectrum management, microwave tomography, and EMC countermeasures.

YOUNG HWAN AHN received the doctor's license, in 1986, and the Ph.D. degree in medicine from Chung-Ang University, Seoul, South Korea, in 2000. In 1991, he became a Neurosurgeon Specialist, and was with the Korean Military Hospital, until 1994. In 1994, he joined the School of Medicine, Ajou University, Suwon, South Korea and Ajou University Hospital, South Korea as a Staff Neurosurgeon, and has been a full-time Faculty Member. Since 2008, he has been conducting research on the biological effects of RF radiation. He is currently the Korean Project Leader of the International Validation Project of the NTP Study on Carcinogenesis of Mobile-Phone Radio-Frequency Radiation. His current research interests include functional neurosurgery and biologic effects of RF-EMF on nervous systems.

KATSUMI IMAIDA received the M.D. and Ph.D. degrees in medical sciences from Nagoya City University, Nagoya, Japan, in 1979 and 1983, respectively. From 1983 to 2000, he was with the Department of Pathology, Nagoya City University. Since 2001, he has been a Professor with Kagawa University, where is currently a Trustee. He has conducted research on the carcinogenesis bioassays. His current research interests include toxicological sciences and carcinogenicities of various chemicals and RF electromagnetic fields.